05,12

Study of magnetic iron oxide nanoparticles coated with silicon oxide by ferromagnetic method

© I.G. Vazhenina[1,2], S.V. Stolyar[2,3], A.V. Tyumentseva[3], M.N. Volochaev[1], R.S. Iskhakov[1], S.V. Komogortsev[1,4], V.F. Pyankov[3], E.D. Nikolaeva[3,5]

[1] Kirensky Institute of Physics, Federal Research Center KSC SB, Russian Academy of Sciences, Krasnoyarsk, Russia
[2] Siberian Federal University, Krasnoyarsk, Russia
[3] Federal Research Center .Krasnoyarsk Science Center of the Siberian Branch of the Russian Academy of Sciences, Krasnoyarsk, Russia
[4] Siberian State University of Science and Technology, Krasnoyarsk, Russia
[5] Krasnoyarsk State Medical University named after Prof. V.F. Voyno-Yasenetsky, Ministry of Health of Russia, Krasnoyarsk, Russia

E-mail: irina-vazhenina@mail.ru

Received April 17, 2023
Revised April 17, 2023
Accepted May 11, 2023.

Magnetic nanoparticles of magnetite with a size of ~ 8 nm synthesized with a different type of coating were studied by ferromagnetic resonance in the temperature range from 7 to 300 K. The features of the experimental temperature dependences of the parameters of the ferromagnetic resonance curve (the magnitude of the resonant field, line width and intensity) and their approximation allowed us to estimate the values of characteristic temperatures. Firstly, the value of the Vervey temperature and the dependence of its value on the type of coating were determined. Secondly, the temperature of transition of nanoparticles to the superparamagnetic state (blocking temperature) and the temperature range within which the magnetic structure of the outer shell of the magnetic nanoparticle is in the spin glass state are established

Keywords: iron oxide nanoparticles, ferromagnetic resonance, superparamagnetism, blocking temperature.

DOI: 10.21883/PSS.2023.06.56095.01H

1. Introduction

Magnetic iron oxide nanoparticles coated with inert materials are promising materials for various applications [1]. They exhibit an optimum ratio between a number of characteristics — sufficiently high magnetization, low chemical activity and good biocompatibility. Recently, these particles have been intensively studied for their application in biomedicine, in particular for cell capture and transfer in magnetic separation.

Magnetic cell separation *in vitro* using magnetic particles is one promising way to obtain individual cell types and subclones from a mixture [2]. An undeniable advantage of this technique is that antibodies bound to magnetic particles can interact with cells in suspension throughout the volume, attaching to them and subsequently entraining them in the magnetic field. In this case, a number of requirements [3,4] to the structure of the antibody nanoparticle. These include, firstly, a preferable range of particle sizes — from hundreds of nanometres to several micrometres, to prevent penetration of the particle into the cell and to maintain a high surface area to volume ratio. Secondly, the mass and magnetic parameters of the nanoparticle (dipole-dipole interaction between individual particles, blocking temperature, magnetic anisotropy of the individual particle) should facilitate its movement within the required separation time and interaction with the cell. Thirdly, the magnetic core requires an inert coating to prevent chemically active iron oxide from affecting cellular processes, and the presence of functionally active groups on the surface of the coating to immobilize antibodies specific to the desired celltype.

The determination of the magnetic parameters of nanoscale powders is often carried out using static methods. In particularly, by measuring the temperature dependences of magnetization in two cooling modes — at zero (ZFC) and at non-zero (FC) magnetic field. The use of nanoparticles in exposure to high-frequency magnetic fields in biomedicine necessitates comprehensive research with both static and dynamic methods [5–7].

This paper presents the results of a study of magnetite nanoparticles by dynamic methods in a wide temperature range.

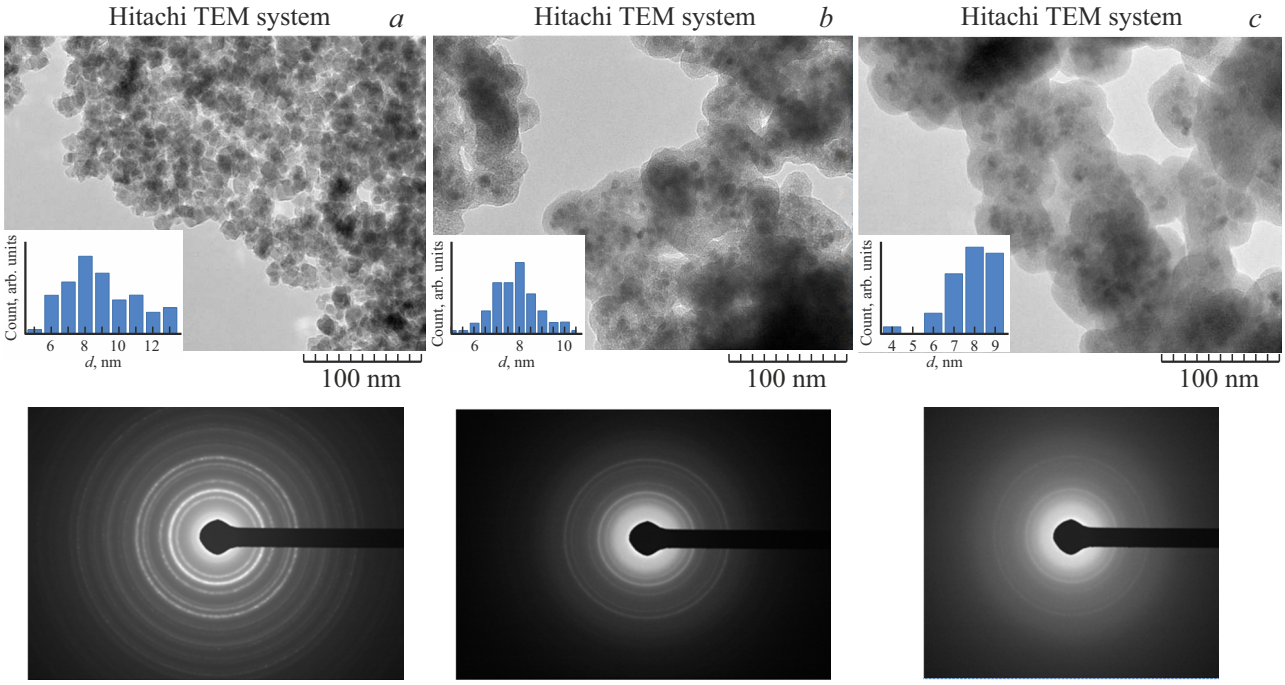

Figure 1. TEM images of magnetic nanoparticles and their size distribution as well as microdiffraction images for uncoated (a), coated with TEOS (b) and double coated with TEOS + APTES (c) powders.

2. Experiment procedure

Magnetic nanoparticles were obtained by chemical co-precipitation of iron salts $FeCl_3$ and $FeCl_2$ in a molar ratio of 2:1 in aqueous solution. For this purpose, 500 mg of the salt mixture was dissolved in 92 ml distilled water and stirred on a mechanical stirrer for 10 min. Then, 8 ml of a 25% aqueous ammonia solution was injected into the solution and incubated under constant stirring for another 30 min. The final pH value after adding aqueous ammonia was 10−11. The resulting magnetic sludge was collected with a neodymium magnet and washed with distilled water to neutral pH (4 fold by 100 μl).

Two types of coating were used to encapsulate the particles. First — single layer silicon oxide coating through the use of tetraethoxysilane (TEOS) in the synthesis process. In the second case, magnetite nanoparticles were coated in two layers — with tetraethoxysilane (TEOS) and 3-aminopropyltriethoxysilane (APTES) — to form a silicate shell containing free amino groups on the surface.

For silicon oxide coating, 20 mg of nanoparticles were suspended in ethanol:water mixture (9:1) and subjected to ultrasonic disaggregation for 3 min. on an ultrasonic sonicator UZTA-0.4/22-OM „Wave“ (Centre for Ultrasound Technology, Russia). 500 μl TEOS was then added drop by drop to the suspension under continuous mechanical stirring. It was incubated at room temperature without stopping stirring, 3 h. The resulting particles were washed three times with distilled water.

Nanoparticles $Fe_3O_4@SiO_2$ with surface amination were synthesized in two steps — coating with tetraethoxysilicate (TEOS) followed by layering with 3-aminopropyltriethoxysilane (APTES) to obtain denser coating and avoid structural deformation by excess NH_2-groups [8].

In the first step, the particles were coated with TEOS according to the protocol described above, but using 350 μl coating material instead of 500 μl. After washing the obtained particles, they were resuspended in a mixture of ethanol:water (ratio 19:1) and under constant stirring at room temperature were added drop by drop to a mixture of 80 μl APTES and incubated for another 20 h to complete the reaction. The particles were then washed three times with distilled water and stored as a suspension in water.

Structural studies were performed on a Hitachi HT7700 TEM transmission electron microscope. The average particle size determined from TEM images is 8 ± 1 nm (Fig. 1).

The ferromagnetic resonance (FMR) curves were recorded on the equipment of Krasnoyarsk Regional Center of Research Equipment of Federal Research Center „Krasnoyarsk Science Center SB RAS“ (ELEXSYS E580 spectrometer, Bruker, Germany) at pumping frequency of resonant cavity $f = 9.48$ GHz (Fig. 2) in the temperature range from 7 to 300 K.

3. Experimental results

The parameters determined from the experimental FMR curves are the resonance field H_R, line width ΔH and

Powder parameters

Cover type, Temperature range	M_S, G	$K_0 \cdot 10^5$, erg/cm^3	Characteristic temperatures, K	
			from fitting $H_A(T)$	from fitting $\Delta H(T)$
Without shell, $7 < T < 100$ K	262	4.0	180	50 and 180
Without shell, $130 < T < 300$ K	193	2.9	240	50 and 220
TEOS, $7 < T < 300$ K	280	2.7	50, 170 and 220	55 and 210
TEOS + APTES, $7 < T < 300$ K	204	2.6	75 and 225	85 and 230

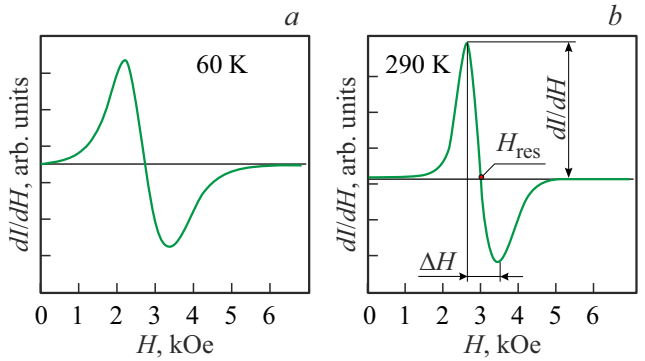

Figure 2. Examples of experimental FMR spectra measured for TEOS coated powders.

intensity *Intensity* equal to $\Delta H \cdot dI/dH$ (Fig. 2, *b*). The temperature dependences of these parameters can be used to estimate the effective magnetization, the anisotropy constant, the degree of particle size homogeneity [9,10]. Also, the experimental values of the resonant field H_R made it possible to determine the field of induced anisotropy $H_A = H_{RS} - H_R$, where H_{RS} — the maximum value of the resonant field, which should coincide with the FMR field of a uniformly magnetized sphere and is equal to ω/γ (γ — the hyromagnetic ratio, $\omega = 2\pi f$). For monodisperse particles, the dependence $H_A(T)$ decreases linearly with temperature, reaching zero at blocking temperature T_B [6,7]. The function $H_A(T)$ we used to describe the experimental values accounted for parameter heterogeneity T_B [11]:

$$\langle H_A(T)\rangle = \langle H_A(0)\rangle \left(\int H_A(T) f(T_B) dT_B\right) / \left(\int f(T_B) dT_B\right), \quad (1)$$

where $\langle H_A(0)\rangle$ — the average H_A with $T = 0$ K. A better agreement with the experimental data (Fig. 3) was achieved by applying a lognormal distribution function T_B:

$$f(T_B) = \frac{1}{T_B \cdot \sigma\sqrt{2\pi}} \exp\left(-\ln\left(\frac{T_B}{T_{B0}}\right)/2\sigma^2\right). \quad (2)$$

T_{B0} value corresponds to a particular magnetic state in the particle magnetic subsystem. It turns out that the number of lognormal modes required to describe the lognormal mode is determined by the type of coverage. T_{B0} values for the samples tested are presented in Table.

The temperature dependence of the ΔH line width of particles with a randomly oriented axis of light magnetization is described by the expression [9,10]:

$$\Delta H(T) = \frac{2}{\sqrt{3}} \frac{\omega}{\gamma} \frac{\alpha(\xi_0 - L_1)}{\xi_0 L_1} + 3\frac{\omega}{\gamma}\frac{\varepsilon L_2}{L_1}, \quad (3)$$

where $\alpha = 0.01$ — attenuation parameter, $\varepsilon = K\gamma/(M\omega)$, K — anisotropy constant, L_1 and L_2 — Langevin functions, $\xi_0 = (\omega/\gamma)(M_S V/k_B T)$, M_S — saturation magnetization, V — particle volume, k_B — Boltzmann constant. The anisotropy constant was described by a function of the form $K(T) = K_0\left(1 + A_0 \exp(-T/T_0) + A_1 \exp(-T/T_1)\right)$. It should be noted that the choice of characteristic temperatures (T_{B0}, T_0 and T_1) in determining the fitting curves of the $H_A(T)$ and $\Delta H(T)$ dependences took into account the points of extremum and inflection on the temperature dependences of the intensity (Fig. 3, *g, h, i*). Expressions (1)–(3) allowed to establish M_S, K_0 and a number of characteristic temperatures (Table).

4. Discussion

$H_A(T)$ and $\Delta H(T)$ functions for uncoated powder were divided into two sections (7 to 120 K and 160 to 300 K) which were considered by separate fitting curves (Fig. 3, *a, d*). The transformation of the $H_A(T)$ dependence observed in the temperature range from 120 to 160 K may be due to a Verwey phase transition. The difference between the temperature of its occurrence as recorded from $H_A(T)$ and that found for natural magnetite (125 K) may be due to deviations in stoichiometry [12]. Each of the lines approximating the dependence $H_A(T)$ of the uncoated powder when extrapolated to its point of intersection with the x axis allows two more characteristic temperatures — 180 and 240 K, which define the blocking temperature of the low and high temperature magnetite phase [6,7]. Comparable characteristic temperature values for this sample were obtained from the $\Delta H(T)$ approximation (Table).

The blocking and Verwey transition temperatures of the encapsulated powders were also estimated using expressions (1)–(3) to describe the dependencies $H_A(T)$ and $\Delta H(T)$. When identifying the characteristic temperatures, it must be taken into account that the additional coating causes an even larger change in the stoichiometry of the outer surface of the nanoparticle and, as a consequence, there is an even larger

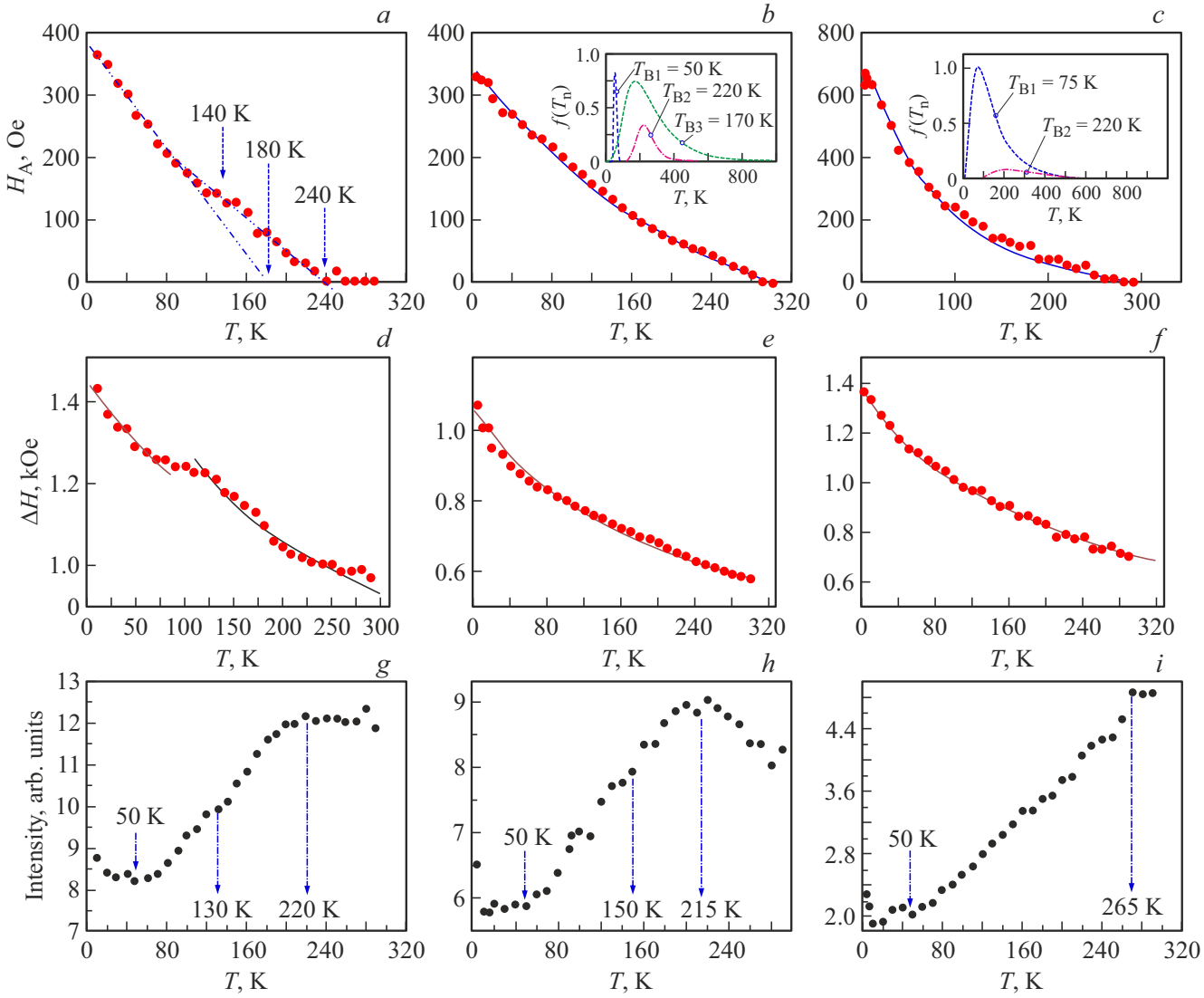

Figure 3. Experimental values (circles) and calculated curves (lines) $H_A(T)$ (a, b, c) and $\Delta H(T)$ (d, e, f) for uncoated powder (a, d, g), coated TEOS (b, e, h) and TEOS + APTES (c, f, i). The inserts show the lognormal distribution functions T_B used when fitting $H_A(T)$. The temperature dependencies of the intensity (g, h, i) are also presented.

shift in the phase transition temperature towards larger values [12]. Thus, the silicon oxide application resulted in a shift of the Verey temperature T_V to 150–170 K, which is fixed by the inflection point on the experimental intensity temperature dependence (Fig. 3, h) and by the characteristic temperature from the approximation curves $H_A(T)$ and $\Delta H(T)$ (Table). The value of T_V with additional APTES coating is not identified by inflection points in the experimental relationships, nor by characteristic temperatures in the approximation. The blocking temperature for either type of coating was determined from the characteristic temperatures of the approximation curves $H_A(T)$ and $\Delta H(T)$ and is 220 ± 10 K. Another characteristic temperature 50 ± 5 K for uncoated powder and powder coated with TEOS and 80 ± 5 K for powder coated with APTES was also identified. We assume that it maps the transition of the nanoparticle surface to a spin glass [7] state.

5. Conclusion

Magnetite nanoparticles with different types of biocompatible coatings were studied by ferromagnetic resonance in the temperature range from 7 to 300 K. The size of the nanoparticles (8 ± 1 nm) and their morphology were determined by electron transmission microscopy. Fitting curves of the experimental values of the anisotropy field H_A and the line width ΔH were obtained assuming a lognormal blocking temperature distribution and an exponential dependence of the anisotropy constant on temperature. The determination of the fitting parameters was carried out

taking into account the extremum points registered in the temperature dependence of the intensity of the FMR curves.

The analytical expressions for $H_A(T)$ and $\Delta H(T)$ allowed the saturation magnetization MS, the effective value of the anisotropy constant K_0, the characteristic temperatures which identify structural and magnetic transformations to be determined. Regardless of the coating type, the transition to the super-paramagnetic state occurs at 210 ± 10 K and the outer shell of the individual nanoparticle is in the spin glass state up to 50 ± 10 K. The encapsulation of magnetite particles with a coating of silicon oxide and NH groups results in a change in Verwey temperature.

Funding

The study was supported by grant No. 22-14-20020 provided by the Russian Science Foundation, Krasnoyarsk Regional Science Foundation.

Conflict of interest

The authors declare that they have no conflict of interest.

References

[1] S.P. Gubin, Y.A. Koksharov, G.B. Khomutov, G.Y. Yurkov. Russ. Chem. Rev. **74**, 489 (2005).
[2] M. Frenea-Robin, J. Marchalot. Magnetochemistry **8**, 11 (2022).
[3] D. Ali, S. Alkahtani, Siddiqui, Alarifi, B.A. Ali. Onco. Targets. Ther. **6**, 75 (2013).
[4] S. Murugadoss, D. Lison, L. Godderis, S. Van Den Brule, J. Mast, F. Brassinne, N. Sebaihi, P.H. Hoet. Arch. Toxicol. **91**, 2967 (2017).
[5] D.A. Balaev, S.V. Stolyar, Y.V. Knyazev, R.N. Yaroslavtsev, A.I. Pankrats, A.M. Vorotynov, A.A. Krasikov, D.A. Velikanov, O.A. Bayukov, V.P. Ladygina, R.S. Iskhakov. Res. Phys. **35**, 105340 (2022).
[6] S.V. Stolyar, R.N. Yaroslavtsev, A.V. Tyumentseva, S.V. Komogortsev, E.S. Tyutrina, A.T. Saitova, Y.V. Gerasimova, D.A. Velikanov, M.V. Rautskii, R.S. Iskhakov. J. Phys. Chem. C **126**, 7510 (2022).
[7] S.V. Stolyar, D.A. Balaev, V.P. Ladygina, A.I. Pankratz, R.N. Yaroslavtsev, D.A. Velikanov, R.S. Iskhakov. Pisma ZhETF **111**, 197 (2020). (in Russian).
[8] Y. Liu, Y. Li, X.-M. Li, T. He. Langmuir **29**, 15275 (2013).
[9] Y.L. Raicher, V.I. Stepanov. ZhETF **102**, 1409 (1992). (in Russian).
[10] I.S. Poperechny, Y.L. Raikher. Phys. Rev. B **93**, 014441 (2016).
[11] S.V. Komogortsev, R.S. Iskhakov, A.D. Balaev, A.V. Okotrub, A.G. Kudashov, N.A. Momot, S.I. Smirnov. Phys. Solid State **51**, 2286 (2009).
[12] A.R. Muxworthy, E. McClelland. Geophys. J. Int. **140**, 101 (2000).

Translated by Ego Translating